TARGET LOCALIZATION IN CELL-BASED IMAGE ANALYSIS AND DISEASE DIAGNOSIS

Noman Saffat Sajid & Md. Shahriar Karim *
Department of Electrical and Computer Engineering, North South University, Dhaka, Bangladesh
{noman.sajid,shahriar.karim}@northsouth.edu

1 INTRODUCTION

Image analysis relying on imaging biological details is integral for disease diagnosis (Caicedo et al., 2017). For example, images collected using fluorescent microscopy require immediate cell profiling and phenotyping, and the segmentation of polyps in organismal scale imaging is also essential. Such objects may hide in the surroundings (Dong et al., 2021) or behave as camouflage (Fan et al., 2020). Although, deep learning (DL) models revolutionized the segmentation of microscopy and medical images (Moen et al., 2019), they have a substantial computational cost. Also, DL models need extensive training data for the available SOTA accuracy, making in-clinic deployment tough. The proposed model identifies the region of interest (ROI) as a bounding circle around the target object, which may facilitate faster training and higher accuracy (Minaee et al., 2021). The object localization scheme localizes the objects of interest in the images, where they are immersed in the background, making the method relevant for various biological and diagnostic goals.

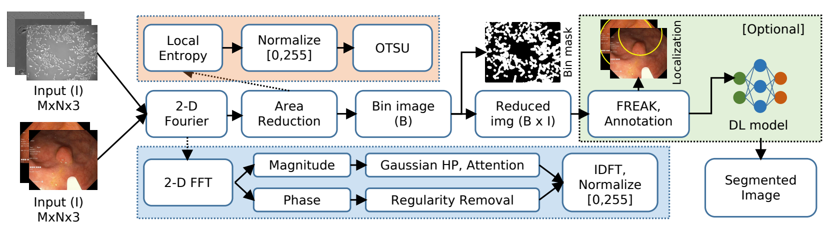

Figure 1: Proposed method for image area reduction and optional bounding circle drawing.

2 MODELS AND METHODS

The proposed method relies on an off-the-shelf approach for image area reduction of microscopy images, localization of camouflage like objects (polyps, tumors, etc.) and draws a bounding circle around the ROI (Fig. 1). Although, localization tasks could be difficult due to the similarity between the object and its surroundings, the proposed method uses common base steps for bounding circle drawing, assuming the background has some regularity as well as variation in intensity with the objects. The method filters the 2-D Fourier transform of the (Oppenheim, 1999)(Smith, 1997) image using Gaussian high pass, followed by a root cubic attention (Pratt, 2013) to enhance the edges of objects. Moreover, the image phase spectrum is normalized to remove the regular regions, that generally make up the background (Aiger & Talbot, 2010). With 2-D IDFT producing the modified image, a normalized version of it is given as the input for the subsequent local entropy analysis. Later, we apply Otsu thresholding (Otsu et al., 1975) to obtain the binary version, which is then used for image area reduction through a pixel wise multiplication with original image. In addition to these base steps, FREAK (Alahi et al., 2012) method generates the keypoints in the reduced image, that we use to draw the bounding circle around the target object. Among the alternative methods tried for keypoints selection, convex hull (Fig. 2e) approach demonstrated the lowest standard deviation. Finally, the center of the convex hull (formed taking 30 lowest keypoints) serves as the center of the bounding circle, drawn by taking the distance of the furthest point as its radius.

*Corresponding author

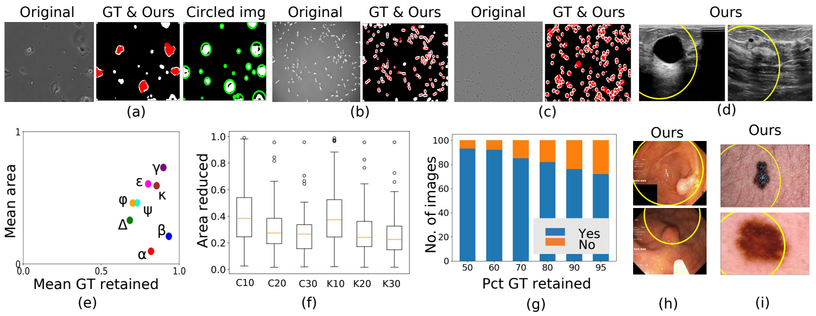

Figure 2: Original image, ground truth (red) superimposed on our method (white) for cell image datasets: (a) PhC-C2DH-U373, (b) PhC-C2DL-PSC, (c) Skbr3. (d) Our method applied on breast cancer images. (e) Mean area vs mean GT retention for 100 randomly taken images on datasets as in part a (α), b (β), c (Δ), Kvasir (κ), CVC-colon (γ), ISIC2016 (ψ), Dermquest (φ), BUSI (ϵ). (f) Area reduced by Convex Hull (C) or K-means (K), using different number of keypoints. (g) 'Yes/No' metric with different amount of GT retained. (h-i) Polyp and skin lesion region localization.

Dataset	PhC-1	PhC-2	SkBr3	Kvasir	CVC-colon	ISIC2016	Dermquest	BUSI
Mean GT	81.8%	93.3%	68.3%	89.8%	85.5%	73.0%	70.2%	80.0%
Area Retained	9.6%	20.9%	33.0%	72.9%	59.2%	46.2%	46.0%	60.5%
Bounding box	Yes	No	No	Yes	Yes	Yes	Yes	Yes

Table 1: Results of our method used on different datasets.

Algorithm 1 Image area reduction Algorithm

Require: N color images
while $i \leq N$ **do**
 $\mathcal{F}(p,q) = \sum_{x=0}^{M-1} \sum_{y=0}^{N-1} I_i(x,y) e^{-j2\pi ux/M} e^{-j2\pi vy/N}$
 $M_{\text{modified}} = \sqrt[3]{|\mathcal{F}(p,q)|_{\text{GHP}}}$
 $P_{\text{modified}} = \mathcal{F}(p,q)/|\mathcal{F}(p,q)|$
 $I_i(x,y)_{\text{Modified}} = \text{Normalize}(\mathcal{F}^{-1}(M_{\text{modified}} \odot P_{\text{modified}}))$
 $I_i(x,y)_{\text{Modified}} = \text{LocalEntropy}(I_i(x,y)_{\text{Modified}}, \text{MorphologicalOperator}_{disk(11)})$
 $I_i(x,y)_{\text{Binary}} = \text{Otsu}(\text{Normalize}(I_i(x,y)_{\text{Modified}}))$
end while

3 Results and Discussion

The efficacy study of the proposed method uses 100 randomly selected images from different datasets (Zargari et al., 2024). As in Fig. 2a-c, the binary mask generated by our method considerably retains the ground truth (GT). In a few datasets, the method retains around 90% of the GT (Table. 1). We also found that a substantial image area reduction is possible maintaining significant overlap with the GT. Together, these suggest that a search of possible tradeoffs between GT overlap and area reduction using the Pareto optimization can further improve the model. Fig. 2d,h,i show a substantial area reduction; however, not in all, as the bounding circle gets large in a few instances. Besides, for over 200 polyp images selected randomly from two datasets, CVC-colon (Silva et al., 2014) and Kvasir-seg (Pogorelov et al., 2017), the drawn bounding circle incorporates 95% of the GT of the polyp in about 73% (Kvasir-seg), indicating the potential of the proposed method in localizing the polyp segmentation task (Fig.2g). We repeated the same experiment for skin lesion and breast cancer dataset (Gutman et al., 2016; Rahman et al., 2024)(see Table 1). Overall, our analysis suggests that off-the-shelf modules in cascade along with local entropy and phase regularity removal, localize objects in diversified datasets, indicating the proposed method's potential to reduce training cost in deep learning models used frequently in the segmentation of cell-based images and images made for medical diagnosis.

Meaningfulness Statement

Imaging-based diagnosis, for example, phenotypical differences between cell populations and colonoscopy, may suffer due to varying shapes, sizes, and the striking similarities between the targets and the image background. In many such applications, deep learning methods are used to segment, profile, and classify microscopy images, but they require extensive training data and computational costs. Our work acquires cell phenotyping data and localizes the targets immersed in an image background. As in the proposed mechanism, a reduced searchable image area can minimize the training cost of deep learning methods, thereby facilitating meaningful and cost-efficient representation of biological phenomena.

References

Dror Aiger and Hugues Talbot. The phase only transform for unsupervised surface defect detection. In *2010 IEEE computer society conference on computer vision and pattern recognition*, pp. 295–302. IEEE, 2010.

Alexandre Alahi, Raphael Ortiz, and Pierre Vandergheynst. Freak: Fast retina keypoint. In *2012 IEEE conference on computer vision and pattern recognition*, pp. 510–517. Ieee, 2012.

Juan C Caicedo, Sam Cooper, Florian Heigwer, Scott Warchal, Peng Qiu, Csaba Molnar, Aliaksei S Vasilevich, Joseph D Barry, Harmanjit Singh Bansal, Oren Kraus, et al. Data-analysis strategies for image-based cell profiling. *Nature methods*, 14(9):849–863, 2017.

Bo Dong, Wenhai Wang, Deng-Ping Fan, Jinpeng Li, Huazhu Fu, and Ling Shao. Polyp-pvt: Polyp segmentation with pyramid vision transformers. *arXiv preprint arXiv:2108.06932*, 2021.

Deng-Ping Fan, Ge-Peng Ji, Guolei Sun, Ming-Ming Cheng, Jianbing Shen, and Ling Shao. Camouflaged object detection. In *Proceedings of the IEEE/CVF conference on computer vision and pattern recognition*, pp. 2777–2787, 2020.

David Gutman, Noel CF Codella, Emre Celebi, Brian Helba, Michael Marchetti, Nabin Mishra, and Allan Halpern. Skin lesion analysis toward melanoma detection: A challenge at the international symposium on biomedical imaging (isbi) 2016, hosted by the international skin imaging collaboration (isic). *arXiv preprint arXiv:1605.01397*, 2016.

Shervin Minaee, Yuri Boykov, Fatih Porikli, Antonio Plaza, Nasser Kehtarnavaz, and Demetri Terzopoulos. Image segmentation using deep learning: A survey. *IEEE transactions on pattern analysis and machine intelligence*, 44(7):3523–3542, 2021.

Erick Moen, Dylan Bannon, Takamasa Kudo, William Graf, Markus Covert, and David Van Valen. Deep learning for cellular image analysis. *Nature methods*, 16(12):1233–1246, 2019.

Alan V Oppenheim. *Discrete-time signal processing*. Pearson Education India, 1999.

Nobuyuki Otsu et al. A threshold selection method from gray-level histograms. *Automatica*, 11 (285-296):23–27, 1975.

Konstantin Pogorelov, Kristin Ranheim Randel, Carsten Griwodz, Sigrun Losada Eskeland, Thomas de Lange, Dag Johansen, Concetto Spampinato, Duc-Tien Dang-Nguyen, Mathias Lux, Peter Thelin Schmidt, et al. Kvasir: A multi-class image dataset for computer aided gastrointestinal disease detection. In *Proceedings of the 8th ACM on Multimedia Systems Conference*, pp. 164–169, 2017.

William K Pratt. *Introduction to digital image processing*. CRC press, 2013.

Md Mostafijur Rahman, Mustafa Munir, and Radu Marculescu. Emcad: Efficient multi-scale convolutional attention decoding for medical image segmentation. In *Proceedings of the IEEE/CVF Conference on Computer Vision and Pattern Recognition*, pp. 11769–11779, 2024.

Juan Silva, Aymeric Histace, Olivier Romain, Xavier Dray, and Bertrand Granado. Toward embedded detection of polyps in wce images for early diagnosis of colorectal cancer. *International journal of computer assisted radiology and surgery*, 9:283–293, 2014.

Steven W Smith. The scientist and engineer's guide to digital signal processing. *California Technical Pub*, 1997.

Abolfazl Zargari, Benjamin R Topacio, Najmeh Mashhadi, and S Ali Shariati. Enhanced cell segmentation with limited training datasets using cycle generative adversarial networks. *Iscience*, 27 (5), 2024.